Article

Cancer Cell

N-Myc Induces an EZH2-Mediated Transcriptional Program Driving Neuroendocrine Prostate Cancer

Graphical Abstract

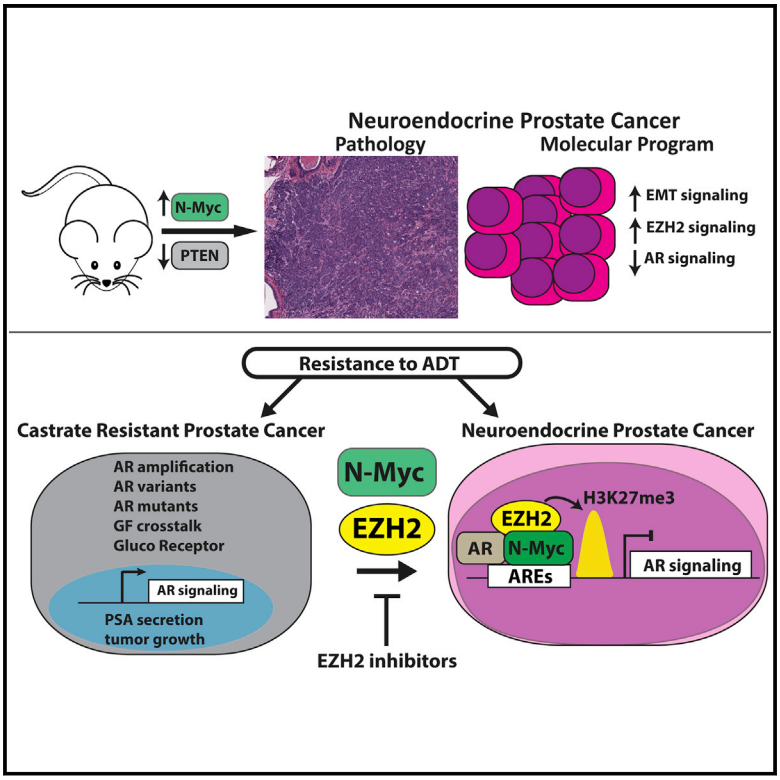

Authors

Etienne Dardenne, Himisha Beltran, Matteo Benelli, ..., Mark A. Rubin, Francesca Demichelis, David S. Rickman

Correspondence

dsr2005@med.cornell.edu

In Brief

Dardenne et al. demonstrate that N-Myc overexpression in pre-clinical models drives aggressive prostate cancer that mimics human neuroendocrine prostate cancer, including reduced AR signaling and enhanced PRC2 target gene repression, and sensitizes cells to an Aurora-A inhibitor and EZH2 SET domain inhibitors.

Highlights

- N-Myc drives the NEPC phenotype and associated molecular program
- N-Myc abrogates AR signaling, which results in enhanced AKT activity
- N-Myc redirects EZH2 activity and sensitizes cells to EZH2 inhibitors
- N-Myc interacts with Aurora-A, which facilitates N-Myc target gene expression

Accession Numbers

GSE86532

Dardenne et al., 2016, Cancer Cell *30*, 563–577
October 10, 2016 © 2016 Elsevier Inc.
http://dx.doi.org/10.1016/j.ccell.2016.09.005

Cancer Cell
Article

N-Myc Induces an EZH2-Mediated Transcriptional Program Driving Neuroendocrine Prostate Cancer

Etienne Dardenne,[1,11] Himisha Beltran,[2,3,4,11] Matteo Benelli,[5] Kaitlyn Gayvert,[6,7] Adeline Berger,[1] Loredana Puca,[4] Joanna Cyrta,[1,4] Andrea Sboner,[1,4,6,7] Zohal Noorzad,[1] Theresa MacDonald,[1] Cynthia Cheung,[1] Ka Shing Yuen,[1] Dong Gao,[8] Yu Chen,[3,8,9] Martin Eilers,[10] Juan-Miguel Mosquera,[1,4] Brian D. Robinson,[1,4] Olivier Elemento,[2,4,6] Mark A. Rubin,[1,2,4,6] Francesca Demichelis,[4,5] and David S. Rickman[1,2,4,12,*]
[1]Department of Pathology and Laboratory Medicine, Weill Cornell Medicine, New York, NY 10065, USA
[2]Meyer Cancer Center, Weill Cornell Medicine, New York, NY 10065, USA
[3]Department of Medicine, Weill Cornell Medicine, New York, NY 10065, USA
[4]Englander Institute for Precision Medicine, New York-Presbyterian Hospital, Weill Cornell Medicine, New York, NY 10065, USA
[5]Centre for Integrative Biology, University of Trento, Trento 38123, Italy
[6]Department of Physiology and Biophysics, Institute for Computational Biomedicine, Weill Cornell Medicine, New York, NY 10065 USA
[7]Tri-Institutional Training Program in Computational Biology and Medicine of Weill Cornell Medicine, Memorial Sloan Kettering Cancer Center, New York, NY 10065, and Cornell University, Ithaca, NY 14853, USA
[8]Human Oncology and Pathogenesis Program, Memorial Sloan Kettering Cancer Center, New York, NY 10065, USA
[9]Department of Medicine, Memorial Sloan Kettering Cancer Center, New York, NY 10065, USA
[10]Theodor Boveri Institute and Comprehensive Cancer Center Mainfranken, Biocenter, University of Würzburg, Am Hubland, 97074 Würzburg, Germany
[11]Co-first author
[12]Lead Contact
*Correspondence: dsr2005@med.cornell.edu
http://dx.doi.org/10.1016/j.ccell.2016.09.005

SUMMARY

The transition from castration-resistant prostate adenocarcinoma (CRPC) to neuroendocrine prostate cancer (NEPC) has emerged as an important mechanism of treatment resistance. NEPC is associated with overexpression and gene amplification of *MYCN* (encoding N-Myc). N-Myc is an established oncogene in several rare pediatric tumors, but its role in prostate cancer progression is not well established. Integrating a genetically engineered mouse model and human prostate cancer transcriptome data, we show that N-Myc overexpression leads to the development of poorly differentiated, invasive prostate cancer that is molecularly similar to human NEPC. This includes an abrogation of androgen receptor signaling and induction of Polycomb Repressive Complex 2 signaling. Altogether, our data establishes N-Myc as an oncogenic driver of NEPC.

INTRODUCTION

Neuroendocrine prostate cancer (NEPC) is a subtype of castration-resistant prostate cancer associated with aggressive clinical features and poor overall survival (Wang et al., 2014). Mounting evidence suggests that NEPC evolves from prostate adenocarcinoma as one mechanism of resistance to androgen receptor (AR)-directed therapies (e.g., abiraterone or enzalutamide). Data from metastatic biopsies obtained from patients progressing on abiraterone or enzalutamide suggests that at least 10% of patients with late-stage castration-resistant prostate adenocarcinoma (CRPC) eventually develop small-cell NEPC

Significance

NEPC is associated with androgen independence and a lack of effective therapeutic options. We demonstrate that N-Myc overexpression in multiple pre-clinical models drives aggressive prostate cancer that molecularly mimics clinical NEPC and sensitizes cells to the allosteric Aurora-A inhibitor MLN8237 and EZH2 SET domain inhibitors. Since transformation to NEPC is thought to develop as a resistance mechanism to androgen receptor (AR)-directed therapies, there is concern that with the clinical development of more potent and earlier AR-targeted therapeutic strategies, the incidence of NEPC may rise. Therefore, findings from this study will impact significantly more prostate cancer patients than previously appreciated and provide rationale for the development of therapeutic strategies for treating this aggressive subtype of prostate cancer.

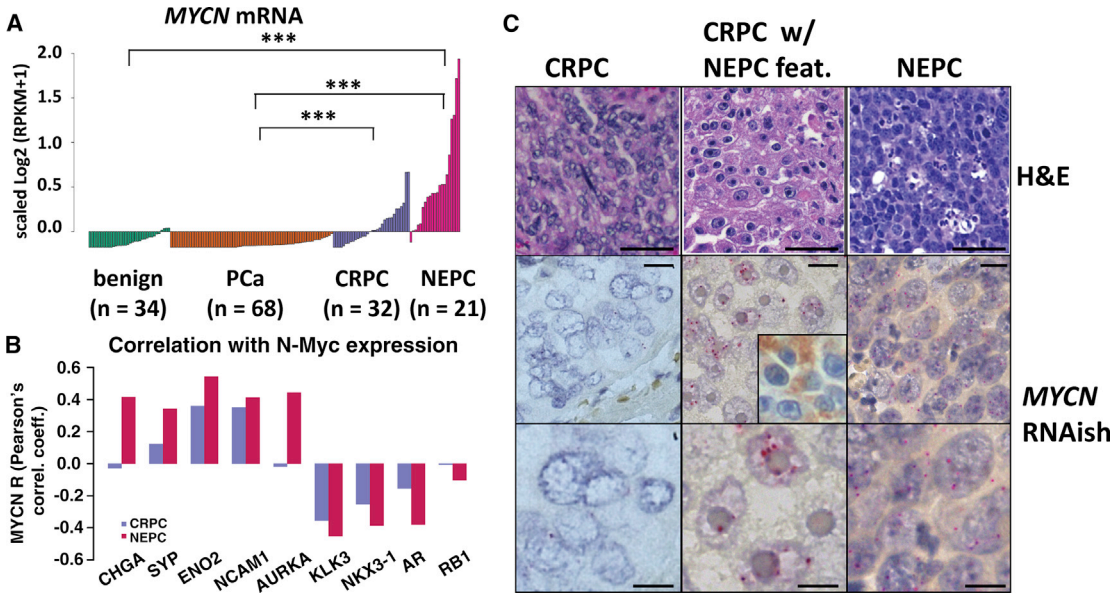

Figure 1. *MYCN* Expression in Prostate Cancer

(A) *MYCN* mRNA level in 34 benign prostate, 68 prostate adenocarcinoma (PCa), 32 castrate-resistant prostate adenocarcinoma (CRPC) and 21 neuroendocrine prostate cancer (NEPC) clinical samples. ***$p < 2.17 \times 10^{-05}$, Wilcoxon test.

(B) Pearson's correlation coefficients between the gene expression level of *MYCN* and AR target genes or neuroendocrine marker genes in CRPC or NEPC samples.

(C) RNA in situ hybridization (RNAish, red chromogen) of *MYCN* RNA in representative CRPC, CRPC with neuroendocrine features (inset: chromogranin A IHC), and NEPC case. Original magnification: 20× for H&E (scale bar, 50 μm, top), and 40× (scale bar, 25 μm, center) and 100× scale bar, 10 μm, bottom) for RNAish. See also Figure S1.

(Small et al., 2016). NEPC tumors share common genomic alterations with CRPC. *ERG* rearrangements and *PTEN* deletions are present in about 50% (Lotan et al., 2011) and 63% (Mosquera et al., 2013; Tan et al., 2014) of NEPC, respectively, and comparable with primary prostate cancer (Cancer Genome Atlas Research Network, 2015) and CRPC (Robinson et al., 2015). The cell plasticity associated with NEPC is associated with decreased or absent expression of the AR and downstream androgen-regulated genes such as prostate-specific antigen (*PSA*). NEPC typically expresses markers of the neuroendocrine lineage (e.g., neuronal-specific enolase (*NSE*), chromogranin A (*CGA*), or synaptophysin (*SYP*)) and is associated with the acquisition of distinct genomic alterations (e.g., *RB1* loss and mutation [Tan et al., 2014] or deletion of *TP53*), epigenomic alterations, dysregulation of specific pathways including neuronal and stem cell programs and epithelial-mesenchymal transition (EMT) (Beltran et al., 2016).

We previously reported significant co-overexpression and gene amplification of *AURKA* (Aurora-A) and *MYCN* (N-Myc) in NEPC tumors (Beltran et al., 2011; Mosquera et al., 2013). Independently of its catalytic activity, Aurora-A forms a complex with and stabilizes N-Myc (Otto et al., 2009), which can be targeted using allosteric Aurora-A inhibitors (Brockmann et al., 2013; Gustafson et al., 2014). In neuroblastoma, the most common extracranial solid cancer in childhood, *MYCN* amplification is an important clinical biomarker and is associated with poor prognosis (Grimmer and Weiss, 2006). We have shown that overexpression of N-Myc in prostate adenocarcinoma cells is associated with the development of neuroendocrine features (Beltran et al., 2011).

To further characterize the functional role of N-Myc as a potential driver of prostate cancer and its role in NEPC, we developed pre-clinical models, including isogenic cell lines, xenografts, genetically engineered mice (GEM), and tumor organoid cultures overexpressing N-Myc.

RESULTS

N-Myc Is Expressed in NEPC and a Subset of CRPC Clinical Samples

We previously reported significant overexpression and gene amplification of *MYCN* in seven NEPCs compared with 30 localized prostate adenocarcinoma (PCa) tumors (Beltran et al., 2011). Based on an extended next-generation RNA sequencing (RNA-seq) dataset (n = 155), we observed that N-Myc is also overexpressed in NEPC (n = 21) compared with CRPC (n = 32) samples (Figure 1A). However, there is a spectrum of N-Myc expression in CRPC samples with 20% (n = 6) of CRPC tumors demonstrating transcript levels in the range of NEPC. We evaluated the AR-signaling status (based on a previously described AR signature; Hieronymus et al., 2006) and NEPC biomarkers across our clinical cohorts, including CRPC and NEPC. In our dataset, high N-Myc expression was associated with, on average, decreased AR and suppressed AR target gene expression (e.g., *KLK3, NKX3.1*) in NEPC as well as in CRPC samples (Figures 1B, S1A, and S1B). We found a consistent difference in the correlation between N-Myc expression and NEPC biomarkers in NEPC compared with that observed in CRPC; Figure 1B shows higher Pearson correlation coefficients

in NEPC for NEPC biomarkers (chromogranin A [*CHGA,* p = 0.04], neuronal-specific enolase [*ENO2,* p = 0.005], neural cell adhesion molecule [*NCAM1,* p = 0.04], Aurora kinase A [*AURKA*, p = 0.03]) and lower coefficients for AR-regulated genes (e.g., prostate-specific antigen [*KLK3*, p = 0.02]) and RB1, as expected. In addition, we found that N-Myc expression is also highly correlated with a recently described molecular classifier of NEPC ($r = 0.63$, $p < 1 \times 10^{-20}$) (Beltran et al., 2016).

To better understand the relationship between N-Myc and the NEPC phenotype at the cellular level, we performed immunohistochemistry (IHC) for N-Myc protein expression in CRPC and NEPC human tissue samples using multiple commercially available N-Myc antibodies. However, none of these antibodies demonstrated sufficient specificity in prostate tissue (data not shown). To overcome this, we developed an in situ hybridization (RNAish) probe for *MYCN* mRNA expression (J.-M.M. and M.A.R., unpublished data). We confirmed abundant levels of *MYCN* mRNA in NEPC tumor cells and in CRPC tumors with focal neuroendocrine differentiation (representative cases are shown in Figures 1C and S1C). Together, these data confirm that N-Myc is abundantly expressed in clinical samples that display an NEPC phenotype. Based on these and earlier pre-clinical findings (Beltran et al., 2011), we hypothesized that N-Myc overexpression is a driver of the aggressive neuroendocrine phenotype in prostate cancer.

N-Myc Overexpression Is Associated with Highly Proliferative, Invasive Prostate Cancer with Neuroendocrine Features

High-grade neuroendocrine carcinomas (e.g., neuroblastoma, NEPC, and small-cell carcinomas of lung and bladder) are aggressive and highly proliferative tumors. To determine if N-Myc increases tumor growth rate, we generated xenografts from 22Rv1 cells with and without N-Myc overexpression. 22Rv1-N-Myc xenografts grew at a significantly higher rate compared with control 22Rv1 xenografts based on cell viability ($p = 0.02$, Student's t test) and, in a larger cohort of mice, based on tumor size ($p = 1 \times 10^{-9}$, Student's t test; Figure S2A). To further determine if N-Myc plays a causal role in driving the NEPC phenotype, we generated GEM mice that carry a CAG-driven lox-stop-lox human *MYCN* gene integrated into the ROSA26 (*LSL-MYCN*) locus (Althoff et al., 2015) and a Tmprss2-driven tamoxifen-activated Cre recombinase (*T2-Cre*; Gao et al., 2016). Within the prostate, T2-Cre specifically mediates Cre recombination in luminal cells (Gao et al., 2016). Since *PTEN* deletion is a frequent alteration in CRPC (50%; Robinson et al., 2015) and phosphatidylinositol 3-kinase (PI3K)/AKT signaling can enhance N-Myc protein stability (Chesler et al., 2006), we also engineered the mice to harbor a *Pten* conditional knockout allele (Chen et al., 2013).

In *T2-Cre*$^{+/+}$;*Pten*$^{f/+}$;*LSL-MYCN*$^{+/+}$ mice, N-Myc was overexpressed in the prostate at 5 weeks after Cre induction by tamoxifen compared with non-induced littermates (Figure S2B), and this was maintained at 3 months post-induction (Figures S2C and S3B). N-Myc overexpression in the context of *Pten*$^{f/+}$ led to focal mouse high-grade prostatic intraepithelial neoplasia (mHGPIN) at 3 and 6 months post-induction (Figure S2D). Non-induced mice or induced littermates that harbor *Pten*$^{f/+}$ alone did not demonstrate mouse PIN at up to 1 year post-induction. In the context of *Pten* null (*Pten*$^{f/f}$), N-Myc expression was associated with diffuse mHGPIN in the ventral and dorsolateral prostate lobes at 3 months post-induction (Figure S3A). The mHGPIN was characterized by the proliferation of cells with nuclear atypia and mitotic figures, expanding throughout the glands, imparting irregular borders, and inducing a mild stromal response and incipient necrosis. Littermates that harbor *Pten*$^{f/f}$ alone also displayed diffuse mHGPIN but were less expansive with more well-defined gland borders and less nuclear atypia. As expected, all *Pten*$^{f/f}$ mice displayed high levels of AKT pathway activity based on phosphorylation of AKT at amino acid S473 (p-AKT; Figure S3D). At 9 months post-induction (*T2-Cre*$^{+/+}$; *Pten*$^{f/f}$; *LSL-MYCN*$^{+/+}$), N-Myc overexpression resulted in large, invasive tumors with a variety of morphologies, including foci of AR-positive adenocarcinoma (Figure S3E) and foci of poorly differentiated carcinoma with divergent differentiation (e.g., intestinal [20% of the tumor], squamous [5%], or sarcomatoid [35%]). The foci of sarcomatoid differentiation were characterized by the presence of atypical spindle cells as well as pleomorphic epithelioid cells, consistent with an aggressive behavior. By IHC, these areas of sarcomatoid differentiation exhibited overexpression of the mesenchymal marker vimentin, an absence of pan-cytokeratin expression, and variable levels of AR expression, suggesting an EMT phenotype. These features have been described in a reconstitution model of NEPC using forward engineered benign human prostate cells (Lee et al., 2016) and of lethal prostate cancer undergoing EMT (Martin et al., 2011), and are rare histologic subtypes in prostate cancer that can arise alone or in the context of classic adenocarcinoma, associated with resistance to hormonal therapy, and carry poor prognosis (Humphrey, 2012; Mott, 1979; Parwani et al., 2004).

Tmprss2 is expressed at low levels in mouse liver (Figure S2B) and starting at 6 months post-tamoxifen induction, *T2-Cre*$^{+/+}$;*Pten*$^{f/f}$;*LSL-MYCN*$^{+/+}$ and *T2-Cre*$^{+/+}$;*Pten*$^{f/+}$;*LSL-MYCN*$^{+/+}$ mice became moribund with massive, multi-focal liver tumors, resulting in a median survival of 117 and 243 days, respectively. Interestingly, these tumors contained small-cell neuroendocrine carcinoma foci in *T2-Cre*$^{+/+}$;*Pten*$^{f/f}$;*LSL-MYCN*$^{+/+}$ liver (Figure S3C). As an alternative, we generated additional N-Myc GEM using the *Pb-Cre4* allele (*Pb-Cre*) (Wu et al., 2001). N-Myc overexpression alone resulted in focal mHGPIN at 12 months of age (Table S1). However, in the context of Pten null N-Myc overexpression (*Pb-Cre*$^{+/-}$;*Pten*$^{f/f}$;*LSL-MYCN*$^{+/+}$), large, intracystic prostatic adenocarcinomas with a variety of morphologies were observed by 3 months of age, including foci of AR-positive adenocarcinoma (Figure 2A), foci of poorly differentiated carcinoma with divergent differentiation (i.e., intestinal, squamous, or sarcomatoid), and foci of more crowded, basophilic cells with more condensed nuclei and less cytoplasm (Figure 2A). In the context of *Pten* heterozygous loss (*Pb-Cre*$^{+/-}$;*Pten*$^{f/+}$;*LSL-MYCN*$^{+/+}$), N-Myc overexpression resulted in large invasive carcinomas with foci containing AR-positive adenocarcinoma, divergent differentiation, or AR-negative NEPC tumor cells at 14 months of age, one of which was observed to have invaded the bladder (Figure 2B). The NEPC foci displayed high levels of *MYCN* RNA based on *MYCN* RNAish at levels similar to what is observed in *MYCN*-amplified

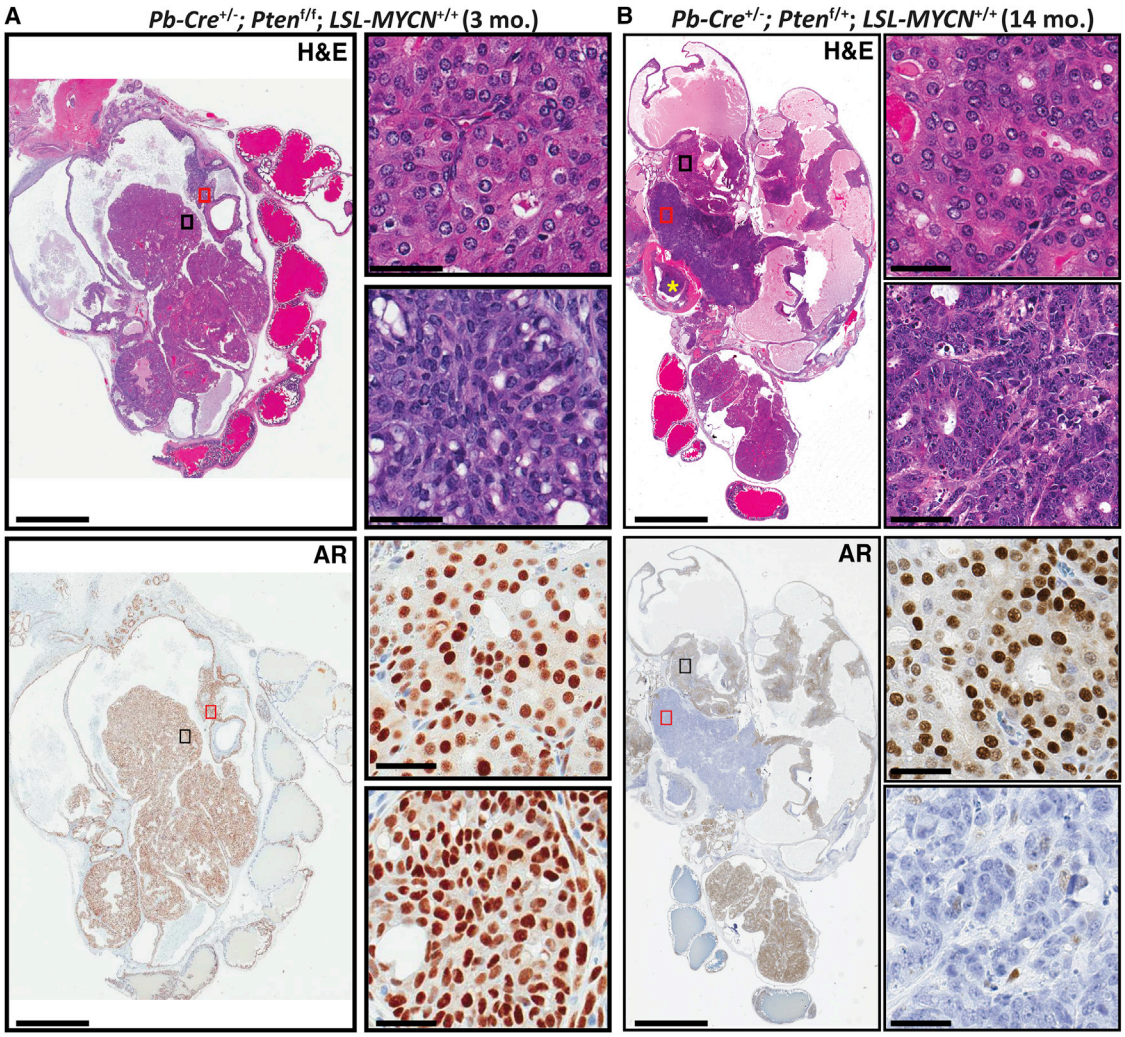

Figure 2. N-Myc Overexpression Is Associated with Aggressive, NEPC-Like Prostate Cancer

(A) Photomicrograph images of H&E stained (top) or AR IHC (bottom) prostate tissue showing AR-positive intracystic carcinoma foci (black rectangle) and AR-positive basophilic foci (red rectangle), at low magnification (left, original magnification 4×; scale bar, 5 mm) and at high magnification (right, original magnification 40×; scale bar, 50 μm); from a 3-month old *Pb-Cre*$^{+/-}$;*Pten*$^{f/f}$;*LSL-MYCN*$^{+/+}$.

(B) Photomicrograph images of H&E stained (top) or AR IHC (bottom) prostate tissue showing invasive, AR-positive adenocarcinoma foci (black rectangle) and AR-negative NEPC foci (red rectangle), at low magnification (left, original magnification 4×; scale bar, 5 mm) with bladder invasion (yellow asterisk) and at high magnification (right, original magnification 40×; scale bar, 50 μm); from a 3-month old *Pb-Cre*$^{+/-}$;*Pten*$^{f/f}$;*LSL-MYCN*$^{+/+}$.

See also Figures S2 and S3 and Tables S1, S2, and S3.

neuroblastoma cases (Figure S2F). Age-matched (14-month *Pb-Cre*$^{+/-}$;*Pten*$^{f/+}$;*LSL-MYCN*$^{-/-}$ and 3-month Pb-Cre; *Pten*$^{f/f}$;*LSL-MYCN*$^{-/-}$) littermates display focal and diffuse mHGPIN, respectively, without divergent differentiation or NEPC features (Figure S2G) consistent with previous studies (Chen et al., 2013), suggesting a role for N-Myc in driving sarcomatoid, intestinal, and neuroendocrine differentiation (Figures S2H–S2K). Interestingly, the foci of intestinal differentiation within the invasive carcinoma demonstrated scattered chromogranin-A-positive cells, which has been reported in a minority (30%–40%) of colon cancers but is seen in all foci of intestinal differentiation in the N-Myc mice (Figure S2K). We did not observe colon cancer at any age in any of the Pb-Cre, N-Myc overexpressing mice. Compared with the roughly 100-week average survival time for *Pb-Cre*$^{+/-}$;*Pten*$^{f/f}$ previously reported (Chen et al., 2013), average survival time for *Pb-Cre*$^{+/-}$;*Pten*$^{f/f}$;*LSL-MYCN*$^{+/+}$ mice was 32 weeks (Figure S2H).

N-Myc Signatures Derived from the N-Myc Mouse and Human Models Are Clinically Representative of NEPC

To determine the clinical relevance of the N-Myc mouse models, we performed RNA-seq from frozen mHGPIN lesions from 3 month post-induction *T2-Cre*$^{+/+}$;*Pten*$^{f/f}$;*LSL-MYCN*$^{+/+}$ or control *T2-Cre*$^{+/+}$;*Pten*$^{f/f}$;*LSL-MYCN*$^{-/-}$ mice. Differential expression analysis identified a set of 918 genes associated with N-Myc expression (779 of those map to human homolog genes; Table S2). Since N-Myc is also overexpressed in a subset of CRPC and to address the clinical relevance of the mouse model,

we used the mouse N-Myc signature to query a combined cohort of 203 well-characterized CRPC and NEPC samples from two published studies (Beltran et al., 2016; Robinson et al., 2015). Hierarchal clustering of the 203 human samples based on the 779 genes segregated the samples into two groups, one of which was significantly enriched with NEPC samples based on pathological criteria, low AR signaling, and high integrated NEPC score from a recently defined multi-gene molecular classifier of NEPC (Beltran et al., 2016) (Figures 3A and S2E, hypergeometric test and Fisher exact test). To determine the generalizability of prostate N-Myc-driven features, we queried neuroblastoma (NB) transcriptomes for the prostate N-Myc signature. Neuroblastoma is a high-grade neuroendocrine tumor, where only a subset of tumors demonstrate high *MYCN* amplification. Based on principal component analysis that included 498 NB samples, the mouse N-Myc signature segregated the neuroblastoma samples according to their *MYCN* amplification status, and the NEPC samples were clustered closer to the *MYCN*-amplified NB samples compared with the non-*MYCN*-amplified NB samples (*MYCN* wildtype; Figure 3B). These findings support N-Myc as a potentially shared driving event in a subset of neuroendocrine cancers.

To determine if N-Myc regulates specific NEPC-associated molecular programs in the mouse model, we performed gene set enrichment analysis (GSEA) using the mouse N-Myc gene expression profile. Importantly, we found that N-Myc overexpression was associated with an induction of EMT genes (false discovery rate [FDR] $q < 1.0 \times 10^{-08}$, e.g., vimentin; Figures 3D, S2K, and S3E and Table S3) and a downregulation of AR signaling (FDR $q < 1.0 \times 10^{-06}$, e.g., *Fkbp5*; Figures 3C and 3D) and of PRC2 target genes (FDR $q < 1.0 \times 10^{-06}$; Figure 3C and Table S3). We also found that the N-Myc signature was enriched with genes associated with *RB1* and *TP53* loss (FDR $q < 4.4 \times 10^{-07}$; Table S3), which are also features of the NEPC molecular program (Beltran et al., 2016; Chen et al., 2012; Tan et al., 2014; Zhou et al., 2006). To determine the robustness of these findings, we generated RNA-seq data from Pb-Cre mouse prostate tissue samples that differ in terms of *Pten* status (two copies, one copy, or null) and that varied in terms the degree of prostate pathology from benign prostate (*Pb-Cre*$^{+/-}$;*Pten*$^{+/+}$;*LSL-MYCN*$^{+/+}$) to invasive prostate cancer (*Pb-Cre*$^{+/-}$;*Pten*$^{f/f}$;*LSL-MYCN*$^{+/+}$). We found that N-Myc drives a molecular signature that is associated with enrichment of PRC2/EZH2 targets, suppression of AR signaling (based on both human AR gene sets and a mouse-defined AR-signaling gene set (Carver et al., 2011)), and upregulation of EMT genes (Figures 3C and 3D and Table S3) across all N-Myc mouse models.

To test these findings in human prostate cancer models, we performed RNA-seq from multiple stable LNCaP or 22Rv1 cell populations overexpressing N-Myc or an empty vector control (Figure S4A). We identified 277 genes for LNCaP +/− N-Myc cells and 1,997 genes for 22Rv1 +/− N-Myc cells that were differentially expressed in the context of N-Myc expression and, as with the mouse RNA-seq data, that were clinically representative (Figure 4A, Table S4, Figures S4B and S4C). GSEA of the LNCaP-N-Myc gene expression profile showed an enrichment of AR-induced genes (e.g., *TMPRSS2, FKBP5, PSA*, GSEA FDR $q = 2.60 \times 10^{-19}$, Table S3), and PRC2 repressed genes (e.g. EZH2 targets, FDR $q = 5.01 \times 10^{-09}$) among the N-Myc downregulated genes. Based on our RNA-seq analysis, we defined a 22Rv1-N-Myc signature that, like the LNCaP N-Myc signature, included N-Myc-downregulated genes significantly enriched with EZH2/PRC2 target genes (FDR $q < 1.4 \times 10^{-12}$) and AR-induced genes (FDR $q < 1.4 \times 10^{-03}$; Figure 4A, Table S2). The N-Myc upregulated genes were enriched with N-Myc target genes in neuroblastoma (FDR $q = 8.97 \times 10^{-82}$), EMT gene sets (FDR $q = 3.9 \times 10^{-05}$; Table S3), embryonic stem cell gene sets (FDR $q = 5.15 \times 10^{-38}$), and genes induced following *RB1* loss (FDR $q = 6.01 \times 10^{-21}$), all of which are molecular features associated with NEPC (Beltran et al., 2011, 2016; Lee et al., 2016). Taken together, N-Myc regulates a molecular program that is consistent between NEPC human tissue samples and our N-Myc prostate cancer mouse model.

N-Myc Reduces AR Signaling

To further characterize the association between N-Myc expression and AR signaling, we generated mouse prostate cancer in vitro models. We adapted a recently reported protocol (Gao et al., 2014; Karthaus et al., 2014) to generate mouse prostate cancer (MPC) organoid cultures from prostates resected from the *T2-CreERT2* inducible or *Pb-Cre*, *Pten* null, +/−*MYCN* GEM mice. Before tamoxifen induction, MPC organoids derived from *T2-Cre*$^{+/+}$;*Pten*$^{f/f}$;*LSL-MYCN*$^{+/+}$ mice were morphologically similar to benign human prostate glands with a luminal and basal cell layer surrounding an empty lumen (Figure S5A). Two weeks after induction, organoids expressed high levels of N-Myc (Figure 5A) and developed a histopathology that resembled tumors observed in the mice (i.e., low number of CK5-positive basal cells, abundant Ki67, and AR-positive luminal cells, some of which are also positive for vimentin; Figures 5B and S5A). Similar to their in vivo tumor counterpart, these organoids also showed lower levels of AR target gene expression (e.g., Tmprss2 and Psca; Figure S5B). *T2-Cre*$^{+/+}$;*Pten*$^{f/f}$;*LSL-MYCN*$^{-/-}$ organoids were also highly proliferative, but unlike *T2-Cre*$^{+/+}$; *Pten*$^{f/f}$; *LSL-MYCN*$^{+/+}$ organoids, they consisted of abundant basal cells. To further test the molecular similarities, we performed RNA-seq analyses on MPC organoids developed from 1.5-month old *Pb-Cre*$^{+/+}$;*Pten*$^{f/f}$;*LSL-MYCN*$^{+/+}$ and *Pb-Cre*$^{+/+}$;*Pten*$^{f/f}$;*LSL-MYCN*$^{-/-}$ mice and found that, as with the GEM prostate tissue, N-Myc drives a molecular signature that is enriched in PRC2/EZH2 targets and suppression of AR signaling (Figure 3C). To determine if *Pb-Cre*$^{+/-}$;*Pten*$^{f/f}$;*LSL-MYCN*$^{+/+}$ organoids display a similar in vivo phenotype as seen in the mouse prostates, we generated organoid allografts by subcutaneously injecting *Pb-Cre*$^{+/-}$;*Pten*$^{f/f}$;*LSL-MYCN*$^{+/+}$ or *Pb-Cre*$^{+/-}$;*Pten*$^{f/f}$;*LSL-MYCN*$^{-/-}$ organoids into immunocompromised mice (n = 17 mice per genotype). We observed bioluminescent-positive tumors in the majority (12 of 17) of *Pb-Cre*$^{+/-}$;*Pten*$^{f/f}$;*LSL-MYCN*$^{+/+}$ 3 months post-injection. As with the GEM tissue, the N-Myc expressing organoid tumors contained adenocarcinoma foci and foci with divergent differentiation (Figure S5C). None of the 17 mice injected with *Pb-Cre*$^{+/-}$;*Pten*$^{f/f}$;*LSL-MYCN*$^{-/-}$ organoids developed tumors up to 3 months post-injection.

To directly test the impact of N-Myc on AR signaling, we treated the in vitro models with either androgen (dihydrotestosterone [DHT]) or an AR inhibitor (enzalutamide) and measured AR target gene expression changes. N-Myc-overexpressing MPC organoids showed lower levels of androgen-induced AR

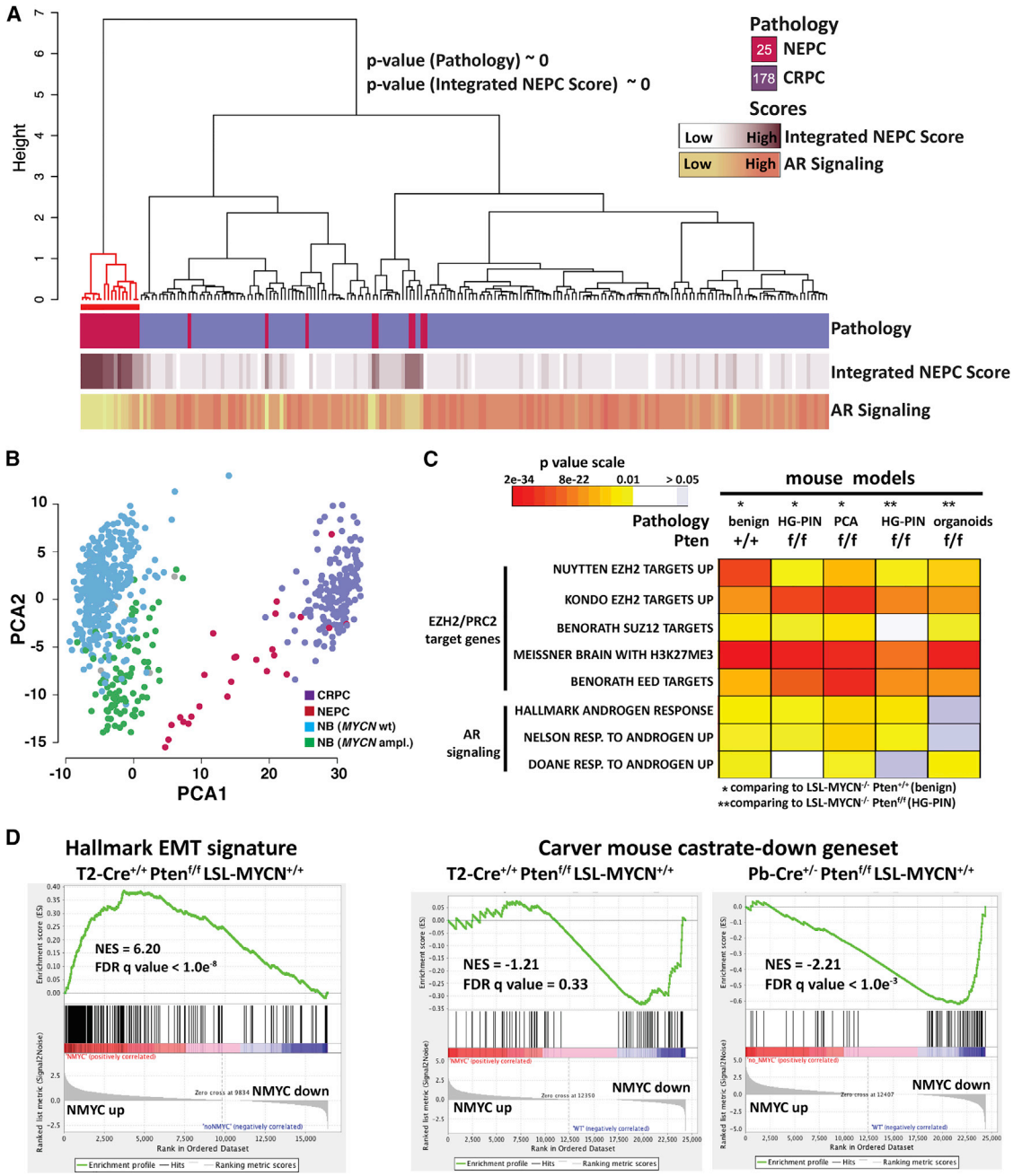

Figure 3. Mouse N-Myc Signature Is Clinically Relevant

(A) Ward's hierarchical clustering of the normalized FPKM values of the 779 prioritized genes across 203 CRPCs samples from two independent cohorts (IPM Cornell, 2011-2015; SU2C-PCF, 2015). Shown p-values result from the hyper-geometric test on CRPC-NE enriched cluster (red color). Pearson's correlation was used as distance measure for samples. Annotation tracks report pathology classification (top), values of integrated NEPC score (middle), and AR signaling (bottom) (darker colors indicate higher scores). The number of samples for each pathology classification is reported inside the square symbols of the corresponding legend. The mouse N-Myc signature segregated the human samples into two groups, one significantly enriched with CRPC-NE samples based on pathological criteria ($p < 10^{-20}$, hypergeometric test) that have high NEPC scores ($p \sim 0$, hypergeometric test).

(B) Projection of the expression levels of the 779 signature genes onto the first and second principal components analysis of the 701 tumor samples RNA-seq data including 498 neuroblastoma (NB) samples (Zhang et al., 2015). Colors indicate tumor classes (CRPC, NEPC, NB with amplified *MYCN*, NB with wild-type [wt] *MYCN*).

(C) Heatmap of GSEA FDR q values of AR-induced genes and multiple PRC2 target gene sets that are significantly enriched in the N-Myc downregulated genes identified in the indicated N-Myc expressing mouse genotypes compared with their non-N-Myc expressing counterparts.

(D) Right: GSEA enrichment plot of the hallmark EMT gene set with the corresponding statistical metrics shown. Left: GSEA enrichment plot of the Carver mouse gene set that represent genes that are downregulated in mouse prostate cancer following castration (Carver et al., 2011).

See also Figure S3 and Tables S2 and S3.

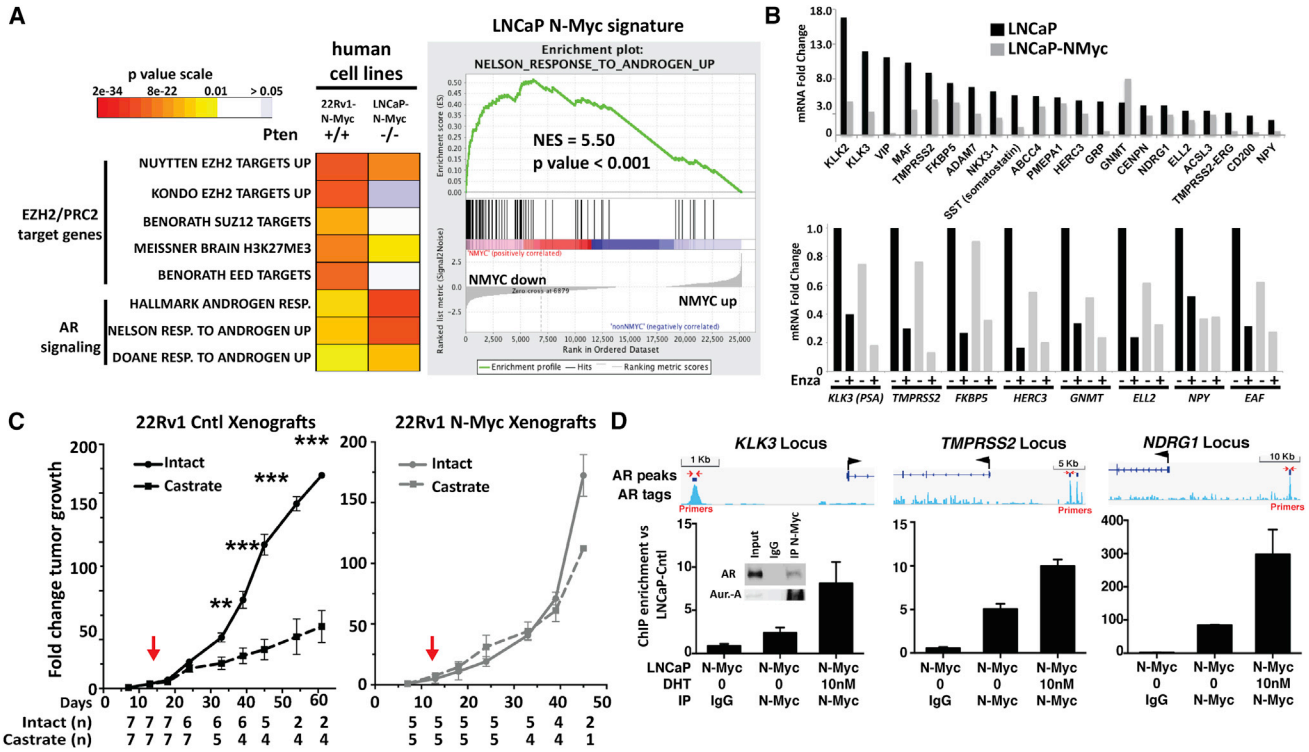

Figure 4. N-Myc Signature in Human Prostate Cancer Cells Is Clinically Relevant and Exhibits a Dramatic Downregulation of AR Signaling

(A) Left: Heatmap of GSEA FDR q values as shown in Figure 3 of AR-induced genes and multiple PRC2 target gene sets that are significantly enriched in the N-Myc de-regulated genes identified in the indicated N-Myc expressing human prostate cancer cell types with the indicated PTEN status compared with their non-N-Myc expressing counterparts. Right: GSEA enrichment plot of the Nelson response to androgen gene set (Nelson et al., 2002) in the ranked N-Myc signature showing the most significantly enriched gene sets.

(B) Nanostring data of AR target gene expression fold induction by androgen (24 hr, 10 nM DHT) in the indicated cell line.

(C) The fold change in growth rate of 22Rv1 control (Cntl, left) or N-Myc (right) xenografts (average ± SEM) in castrated (dashed lines) or intact (solid lines) mice (red arrow indicates the time at which the mice were castrated). Each tumor size at each time point was normalized to values obtained at 1 week before the day of castration (**p = 0.003, ***$p < 10^{-7}$, Student's t test).

(D) ChIP-PCR for N-Myc at known AR enhancers for indicated genes following 48 hr growth in charcoal stripped serum with or without 24 hr of 10 nM DHT (inset: Co-IP of N-Myc from LNCaP-N-Myc cells showing the interaction between N-Myc and AR and Aurora-A as a positive control). See also Figure S4 and Tables S3, S4, and S5.

target gene induction and were less responsive to enzalutamide (p = 0.002, Student's t test; Figure 5C). These findings were confirmed in the LNCaP-N-Myc cells. Using a targeted multiplex qRT-PCR assay (J.-M.M. and H.B., unpublished data; Beltran et al., 2016) that assesses AR signaling, we found that LNCaP-N-Myc cells displayed a dramatic abrogation of AR signaling following DHT treatment compared with LNCaP-cntl cells (Figure 4B, top). As observed in the organoids, LNCaP-N-Myc cells treated with enzalutamide showed a further reduction of some AR target genes compared with LNCaP-cntl cells (Figure 4B, bottom). To determine if the overexpression of N-Myc induces a faster recurrence in the context of castration, we compared the 22Rv1 xenograft tumor growth rate in the context of intact or castrated mice. 22Rv1 control cells, which are derived from a CRPC metastatic lesion, grew at a slower rate as xenografts in castrated mice compared with intact mice beginning 20 days post-castration (p = 0.0002, Student's t test) and continued until the end of the experiment ($p = 1 \times 10^{-22}$, Student's t test). 22Rv1-N-Myc xenografts grew at the same rate in intact and in castrated mice throughout the experiment (Figure 4C) with the majority of tumors reaching maximal acceptable size as per Weill Cornell Medicine (WCM)-Institutional Animal Care and Use Committee (IACUC) standards.

From the mouse and human cell line data, N-Myc overexpression was associated with decreased AR signaling. Given the tendency for lower AR levels in N-Myc CRPC samples, we queried AR levels in the mouse models. We observed robust nuclear expression of AR throughout the mHGPIN lesions that displayed high levels of *MYCN* mRNA as determined by IHC, similar to N-Myc negative control prostate tissue (Figures S3 and S2). This suggests that N-Myc may affect AR signaling not by altering AR levels in the nucleus but rather by binding directly at the sites of target genes to repress transcription and/or blocking AR binding at AR enhancers. Based on targeted chromatin immunoprecipitation (ChIP)-PCR, we did not observe a significant change in androgen-induced AR binding at specific AR enhancer sites in the context of N-Myc overexpression (Figure S4D). However, we found that N-Myc and AR physically interact and that N-Myc also binds at these AR enhancers (Figure 4D). Interestingly, N-Myc binding at AR enhancers was

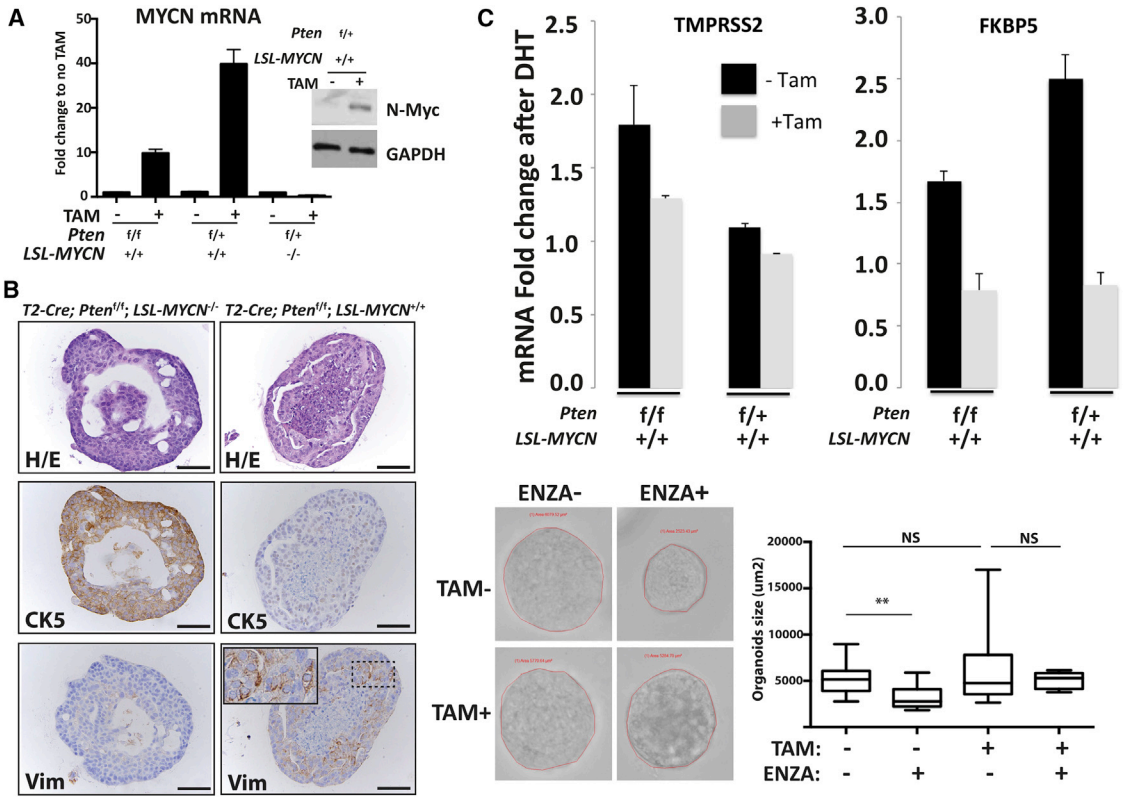

Figure 5. MPC Organoids Culture Mimic In Vivo Mouse Features

(A) RT-qPCR and western blot analysis from MPC organoids showing N-Myc mRNA and protein expression with or without 2 weeks of tamoxifen induction.

(B) Photomicrographs (scale bar, 50 μm) of representative mouse prostate organoids from the genotype mouse indicated following H&E staining, cytokeratin 5 (CK5), and vimentin (Vim) IHC staining. Inset: higher magnification of dashed box.

(C) RT-qPCR data of mRNA levels of the indicated AR target genes from organoids 3 weeks with or without tamoxifen and following 1 day stimulation with 10 nM DHT. Shown are average and SD fold change compared with vehicle-treated organoid cultures (n = 3 independent organoid cultures). Below: *T2-Cre*$^{+/+}$;*Pten*$^{f/f}$;*LSL-MYCN*$^{+/+}$-derived prostate organoids with and without tamoxifen organoids culture were seeded for 48 hr and then treated with enzalutamide (1 μM) for 72 hr and the surface area of each organoid was calculated. Boxplot representation of the surface area distribution of the organoids (n > 15 organoids per condition). Enzalutamide reduced the surfaced area of the control organoids but did not have a significant effect on N-Myc-expressed organoids. **p = 0.0021, Student's t test.

See also Figure S5 and Tables S2 and S3.

observed in the absence of DHT and was enhanced by the presence of DHT, suggesting that N-Myc binding at the enhancers occurs in the absence of AR and is stabilized by its interaction with AR or another interacting cofactor. No N-Myc binding was observed at a control region in the *CDH5* locus (Figure S4C). nMotif analysis at these 175 base pair AR enhancer regions shows that two of the three enhancers contain N-Myc binding motifs, defined by reported N-Myc motifs in MotifDB or non-canonical E-Boxes CANNTG motifs (Table S5).

One N-Myc downregulated AR target is FKBP5, a scaffolding protein for AKT and PHLPP that promotes PHLPP dephosphorylation of AKT at amino acid S473 (Brognard et al., 2007; Ratajczak et al., 2003) and mediates AR-AKT pathway crosstalk (Carver et al., 2011; Mulholland et al., 2011). We found that N-Myc expression is associated with enhanced AKT signaling based on p-AKT protein levels in LNCaP cells (Figures 6A and S6), transgenic mouse prostates (p-AKT IHC in mHGPIN lesions Figure S2), and mouse-derived organoids (Figure 6B). Further, N-Myc expression sensitizes cells and organoids to the PI3K/AKT pathway inhibitors BKM120 and BEZ235 (Figures 6A and 6B). PI3K/AKT signaling has previously been shown to enhance N-Myc protein stability in neuroblastoma by blocking GSK3β phosphorylation of N-Myc at T58 (Chesler et al., 2006). Therefore, we reasoned that AKT pathway inhibition with different inhibitors (Figure S6B) should also lower N-Myc levels in our model systems. Treatment of LNCaP-N-Myc cells with BEZ235, BKM120, RAD001, or MK2206 resulted in decreased N-Myc levels after 6 hr (Figure S6C). To further define the mechanism involved in N-Myc and PI3K/AKT regulation, we determined FKBP5 levels and the ratio of T58 phosphorylated N-Myc to total N-Myc (T58-N-Myc/N-Myc) following PI3K pathway inhibition. BEZ235 treatment resulted in a decrease in steady-state levels N-Myc, an increase in the T58-N-Myc/N-Myc ratio, and a concomitant restoration of FKBP5 protein levels (Figure S6C) in LNCaP-N-Myc, arguing that this pathway is intact in N-Myc overexpressing prostate cancer.

N-Myc Forms a Complex with EZH2

EZH2 and N-Myc are both overexpressed in a subset of CRPCs and in the vast majority of NEPCs (Figure S7A) (Beltran et al.,

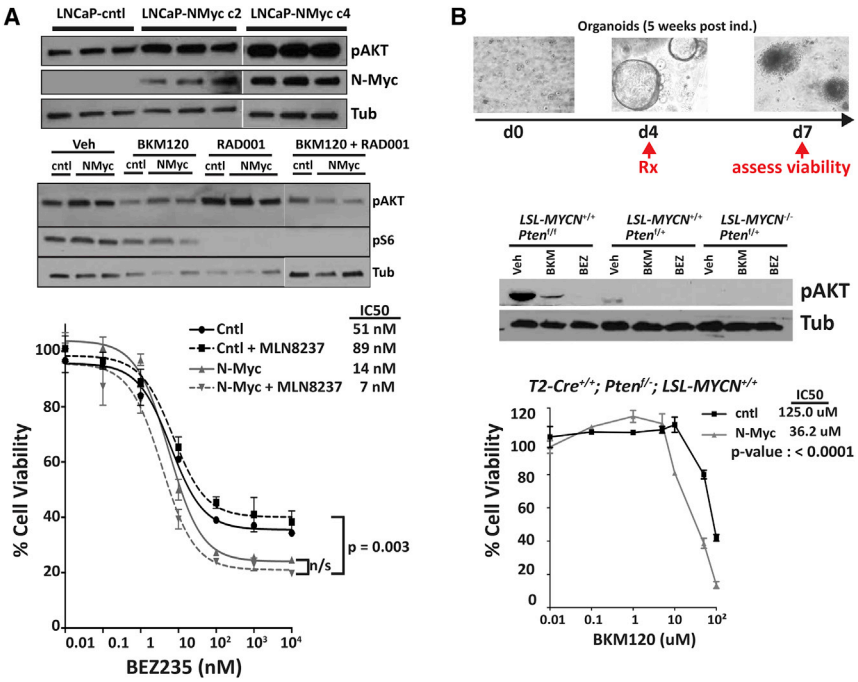

Figure 6. N-MYC Increases AKT Signaling in Cell Line and Organoids

(A) Western blot analysis of p-AKT in LNCaP-N-Myc cells compared with LNCaP-cntl (upper panel). Western blot analysis of p-AKT and phospho-S6 ribosomal protein (Ser235/236) in LNCaP-N-Myc cells compared with LNCaP-cntl, 24 hr after treatment with BKM120 (1 μM) and RAD001 (100 nM) alone or in combination (middle panel). Dose-response following 72-hr incubation with the indicated dose of BEZ235 obtained for LNCaP-N-Myc cells and LNCaP-cntl and in the presence or absence of MLN8237 (100 nM) (lower panel).

(B) Drug treatment in prostate organoids culture. Top: experiment design; below: western blot analysis of p-AKT after 48 hr of BKM120 (1 μM) and BEZ235 (100 nM) treatment. Bottom: dose-response of BKM120 for *T2-Cre*$^{+/+}$;*Pten*$^{f/+}$;*LSL-MYCN*$^{+/+}$ organoid culture compared with the non-induced organoids.

See also Figure S6.

2016). In addition, the N-Myc signatures in the mouse and LNCaP model systems are enriched with PRC2 target genes. N-Myc interacts with AR, and EZH2 has also been shown to interact with AR (Xu et al., 2012). Therefore, we sought to determine if there is a relationship between N-Myc and EZH2 signaling. We observed high levels of EZH2 protein and EZH2 activity (based on histone 3, lysine 27 tri-methylation [H3K27me3] IHC) in *Pb-Cre*$^{+/-}$;*Pten*$^{f/f}$;*LSL-MYCN*$^{+/+}$ mice at 6 months compared with the low levels observed in control mouse prostates (Figure 7A and S7B). In addition and based on co-immunoprecipitation assays, we found that N-Myc interacts with EZH2 and the PRC2 component SUZ12 (Figure 7B). Interestingly, we also found that the N-Myc/AR interaction depends on the presence of EZH2 based on siRNA directed knockdown of EZH2. In order to test if the catalytic activity of EZH2 is essential for complex formation, we performed N-Myc co-immunoprecipitation following the introduction of a previously described SET domain-deletion EZH2 mutant (Xu et al., 2012). Although N-Myc interacts with the mutant EZH2 (Figure S7C), treatment with the catalytic inhibitors GSK126 or GSK343 reduced the interaction between N-Myc and EZH2 and between N-Myc and AR (Figure 7B). Moreover, consistent with the SUZ12-EZH2 interaction (Kim et al., 2015), we found that the N-Myc interaction with SUZ12 is also sensitive to EZH2 catalytic inhibition. Altogether, these results suggest that the catalytic activity of EZH2 enhances N-Myc/AR/EZH2-PRC2 complex formation.

Since EZH2 is a histone methyltransferase and acts as part of the PRC2 to repress gene transcription, we hypothesized that EZH2 cooperates with N-Myc in downregulating the expression of N-Myc target genes. To address this, we performed RNA-seq analyses in LNCaP-N-Myc cells following either siRNA-mediated EZH2 knockdown or treatment with GSK343 in replicate (correlation between replicates is r = 0.95) and monitored the impact of either condition on N-Myc target gene expression compared with siRNA control or vehicle treatment, respectively. Plotting the rank order of the genes upon EZH2 knockdown or GSK343 treatment, we found that N-Myc downregulated N-Myc target genes were significantly upregulated (Figure 7C). Further GSEA analysis and hypergeometric tests of the N-Myc downregulated genes that are upregulated ($\log_2$[fold change] < 0.5) upon either EZH2 knockdown or GSK343 treatment compared with control conditions revealed a significant enrichment of AR-induced genes and PRC2/EZH2 target genes (Figures 7C and S7D), suggesting that EZH2 inhibition reverses N-Myc gene regulation. To test this, we assessed the histone methytransferase activity of EZH2 in LNCaP cells +/− N-Myc overexpression by performing H3K27me3 ChIP-seq. We found a statistically significant difference ($p = 0.047$) between the relative levels of H3K27me3 marks at the promoters of the N-Myc downregulated genes between LNCaP-N-Myc cells compared with control cells. GSEA hypergeometric tests of N-Myc-specific H3K27me3 peaks revealed a significant enrichment of AR-signaling genes (gene sets: Hallmark AR response, $q = 1.02 \times 10^{-11}$; Nelson response to AR up, $q = 4.61 \times 10^{-8}$) and EZH2 targets (gene sets: Nuytten EZH2 targets up, $q = 1.24 \times 10^{-6}$). Targeted EZH2 and H3K27me3 ChIP-PCR at specific AR-binding sites confirmed the increased EZH2 binding and catalytic activity in the context of N-Myc overexpression (Figure 7D). Altogether, our RNA-seq and ChIP-seq data support a model of EZH2 acting as a co-repressor with N-Myc to drive the NEPC molecular program.

Treatment of LNCaP cell lines with EZH2 inhibitors lowered H3K27 global methylation irrespective of N-Myc status (Figure S7C). However, N-Myc overexpression resulted in a higher sensitivity to EZH2 inhibitors GSK126 or GSK503 in LNCaP or 22Rv1 isogenic cells, respectively, compared with control cells lacking N-Myc (Figure 7E). To determine if the N-Myc-associated enhanced sensitivity to EZH2 inhibitors is observed in vivo, we treated mice harboring isogenic 22Rv1

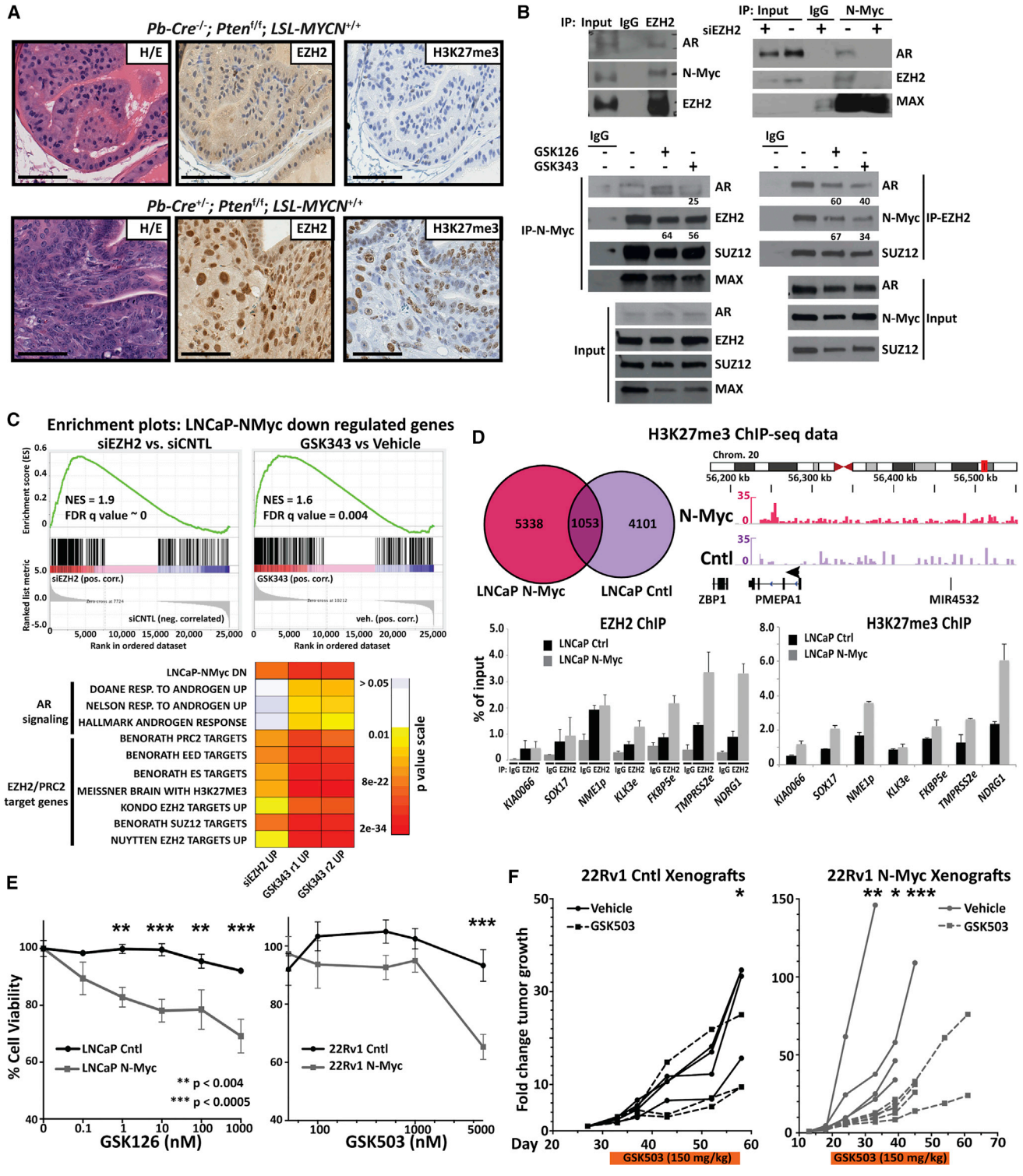

Figure 7. N-Myc Interacts with EZH2 to Drive the Transcriptional Program

(A) Photomicrographs of representative mouse prostates from the indicated genotype following H&E staining, EZH2, and H3K27 tri-methylation (H3K27me3) IHC staining (scale bar, 50 μm).

(B) Co-immunoprecipitation of N-Myc, EZH2, SUZ12, and AR upon EZH2 or N-Myc pull-down in LNCaP-N-Myc cells and in LNCaP-N-Myc cells following knockdown of EZH2 with siRNA targeting EZH2 mRNA (top center), transfection of the Myc-tagged SET domain-deletion EZH2 mutant (top right), or 6-day treatment of either the EZH2 inhibitors GSK126 or GSK343 (bottom). Values below indicate the percent of interaction compared with vehicle if below 70%.

(legend continued on next page)

xenografts (+/− N-Myc overexpression) with the EZH2 catalytic SET domain inhibitor GSK503 at 150 mg/kg daily or vehicle for 32 days. Mice harboring control 22Rv1 xenografts showed little to no response to treatment compared with vehicle up to day 25 post-treatment (average tumor size, 29.6 cm^3 [vehicle] versus 14.9 cm^3 [GSK503], $p = 1.0 \times 10^{-6}$, Student's t test) and were sacrificed on day 31 due to reaching maximal tumor size as per WCM-IACUC standards (Figure 7F). On the other hand, the N-Myc overexpressing xenografts showed a statistically significant 5-fold difference in tumor growth in the treatment group compared with vehicle as early as day 11 post-treatment (average tumor size, 57.6 cm^3 [vehicle] versus 10.1 cm^3 [GSK503], $p = 5.8 \times 10^{-4}$, Student's t test), which was maintained until the end of the treatment (32 days post-treatment, average tumor size, 109.0 cm^3 [vehicle] versus 26 cm^3 [GSK503], $p = 3.0 \times 10^{-4}$, Student's t test). No weight loss was noted for any of the GSK503 treated mice over the course of the experiment.

N-Myc Forms a Targetable Complex with Aurora-A that Facilitates N-Myc Target Gene Expression

Consistent with neuroblastoma, N-Myc and Aurora-A interact to form a complex that results in N-Myc and Aurora-A stabilization in NEPC (Beltran et al., 2011). Although the catalytic activity of Aurora-A is not required for stabilizing N-Myc (Otto et al., 2009), the interaction of N-Myc with Aurora-A is disrupted by a class of allosteric Aurora-A inhibitors (e.g., MLN8237; Brockmann et al., 2013; Gustafson et al., 2014). In LNCaP-N-Myc cells, treatment with MLN8237 led to a rapid dissociation of N-Myc from Aurora-A and promoted degradation of N-Myc based on measurements of steady-state levels and a fluorescent protein-protein proximity ligation assay that assesses N-Myc/Aurora-A complex in isogenic cell lines (Figures 8A and 8B). Moreover, N-Myc overexpressing cells displayed an enhanced sensitivity to MLN8237 in terms of cell viability in cell lines (LNCaP-N-Myc median inhibitory concentration [IC_{50}] = 24.3 nM; LNCaP-cntl IC_{50} = 2.015 nM; Figure 8C) and in organoids (*T2-Cre$^{+/+}$;Pten$^{f/f}$;LSL-MYCN$^{+/+}$* IC_{50} = 25.6 μM; *T2-Cre$^{+/+}$;Pten$^{f/f}$;LSL-MYCN$^{-/-}$* IC_{50} = 47.5 μM; Figure 8D). Since the organoids are grown in three-dimensional cultures that include Matrigel, higher overall doses are needed. MLN8237 also leads to a decrease in N-Myc target gene expression (e.g., *PEG10* and vimentin; Figure 8E). Based on our finding that N-Myc overexpressing cells are more sensitive to PI3K/AKT pathway inhibitors, we combined an AKT inhibitor with MLN8237. Although it did not reach statistical significance, the combination of MLN8237 with BEZ235 yielded the lowest IC_{50} (Figure 6).

DISCUSSION

NEPC rarely arises de novo, and is most commonly diagnosed in later stages of prostate cancer progression. In these cases, the clonal evolution of NEPC from prostate adenocarcinoma distinguishes it from small-cell neuroendocrine carcinomas arising from other primary sites (Beltran et al., 2011; Beltran et al., 2016; Lotan et al., 2011; Scheble et al., 2010; Williamson et al., 2011). Since transformation of NEPC is thought to develop as a mechanism of resistance to hormonal therapy (Ito et al., 2001; Shen et al., 1997; Wright et al., 2003; Yuan et al., 2006), there is concern that with the clinical development of more potent and earlier AR-targeted therapeutic strategies, the incidence of NEPC could escalate. We previously reported that *MYCN* amplification and overexpression are common in NEPC (Beltran et al., 2011; Mosquera et al., 2013).

To characterize the functional role of N-Myc as a driver of prostate cancer, we developed unique N-Myc transgenic mouse lines, MPC organoids, and cell line models. Based on histopathological and molecular data, N-Myc overexpression was associated with an induction of the NEPC histological phenotype and molecular program. While this study was in review, Lee et al. (2016) reported highly complementary results using a forward engineering approach of benign human prostate cell that overexpress N-Myc in the context of myristoylated AKT. In that study, Lee et al. (2016) provided compelling data showing that N-Myc overexpression resulted in castrate-resistant tumors with NEPC or adenocarcinoma histology foci. Foci showing divergent differentiation were also observed. These complementary results solidify N-Myc as a driver of the NEPC phenotype.

In our models, N-Myc abrogates AR signaling and enhances PRC2 target gene repression irrespective of Pten status or the degree of prostate pathology. We found that N-Myc overexpression desensitizes MPC organoids and xenografts to AR antagonist therapy or castration, respectively. The N-Myc transcriptional program also included an enrichment of upregulated gene sets associated with stem cells (FDR $q = 1.02 \times 10^{-02}$), cell migration (FDR $q = 2.64 \times 10^{-03}$), and neural programs (FDR $q = 4.69 \times 10^{-03}$). It was also enriched with signaling signatures associated with RB1 and TP53 loss, genomic alterations enriched in NEPC (Beltran et al., 2016; Chen et al., 2012; Tan et al., 2014; Zhou et al., 2006). Interestingly, expression of N-Myc in the liver of *T2-Cre$^{+/-}$;Pten$^{f/f}$;LSL-MYCN$^{+/+}$* mice

(C) Top: GSEA enrichment plot of the N-Myc downregulated gene set in genes ranked in terms of comparison of LNCaP-N-Myc cells treated with siRNA targeting EZH2 versus control siRNA or GSK343 versus vehicle treatment. Bottom: heatmap of GSEA FDR q values as shown in Figure 3 of AR-induced genes and multiple PRC2 target gene sets that are significantly enriched in the N-Myc downregulated genes that were significantly upregulated after either siRNA-mediated EZH2 knockdown (48 hr) or treatment with GSK343 (7 days, 5 μM) in replicate.

(D) Top left: Venn diagram showing the overlap between H3K27me3 ChIP-seq reads enriched at promoters either in LNCaP-N-Myc or control (Cntl) cells. Top right: H3K27me3 ChIP-seq reads in the indicated cells that were localized at the chromosome loci housing the AR-regulated gene *PMEPA1*; bottom: EZH2 ChIP-PCR at known EZH2-binding sites for the indicated EZH2 target gene or negative control gene (*KIA0066*).

(E) Left: percent cell viability of either LNCaP control (Cntl) or LNCaP-N-Myc (N-Myc) cells following 6 days incubation of the indicated dose of the EZH2 inhibitor GSK126.

(F) The fold change in growth rate of individual 22Rv1 control (Cntl, left) or N-Myc (right) xenografts before, during (orange bar below), and after 31 or 35 days (respectively) treatment with 150 mg/kg of the EZH2 inhibitor GSK503 (dashed lines) or vehicle (solid lines). Each tumor size at each time point was normalized to values obtained at day 1 of treatment. *p = 0.03, **p = 0.0006, ***p = 0.0003, Student's t test.

See also Figure S7.

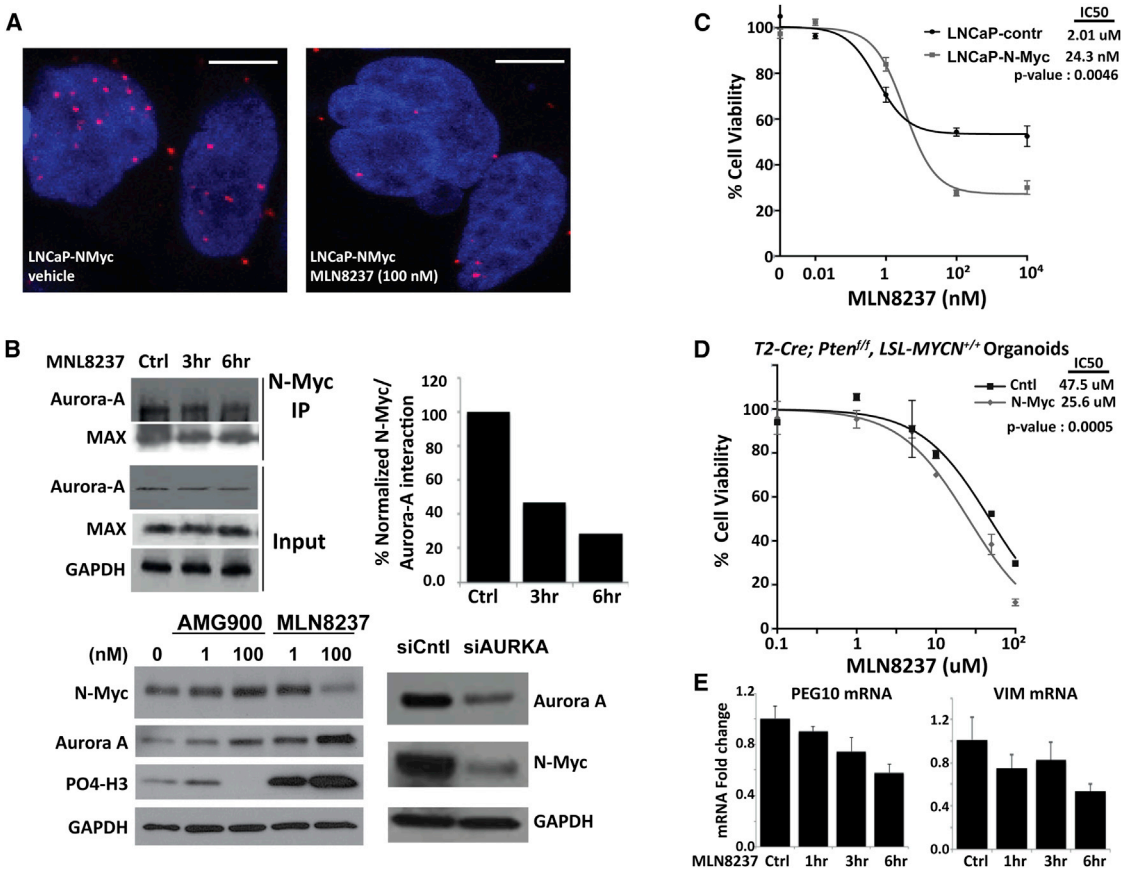

Figure 8. N-Myc/Aurora-A Complex Is Targetable with Allosteric Aurora-A Inhibitors, e.g., MLN8237

(A) Proximity ligation assay (PLA) for the N-Myc/Aurora-A complex. Each red dot represents an interaction (scale bar, 5 μm). Below: representative images of a PLA assay in LNaP-N-Myc cells treated with either vehicle or 100 nM MLN8237 for 48 hr.

(B) Western blot analysis of N-Myc in LNCaP-N-Myc cells following treatment with the indicated Aurora-A inhibitors at the indicated dose or siRNA targeting *AURKA* mRNA for 48 hr.

(C) Dose-response data are shown for the same cells shown in the western blot.

(D) Organoid culture viability assay after increasing doses of Aurora-A inhibitor MLN8237. Shown are average and SD fold change compared with vehicle-treated organoid cultures (n = 3 independent organoid cultures).

(E) RT-qPCR of *PEG10* and vimentin (*VIM*) mRNA after a time course of MLN8237 (1 μM) treatment.

displayed hepatocellular carcinoma foci (similar to what has been observed in c-Myc amplified human and mouse models of liver cancer; Schlaeger et al., 2008; Shachaf et al., 2004) but also small-cell neuroendocrine carcinoma, which had not been reported in c-Myc models. Small-cell liver carcinoma has been described but is extremely rare (Khaw et al., 2011) and to date has not been linked to N-Myc overexpression. Therefore, *T2-Cre*$^{+/-}$*;Pten*$^{f/f}$*;LSL-MYCN*$^{+/+}$ mice provide a potential model to study this rare liver tumor type. Altogether, these data reinforce the idea that N-Myc can drive a neuroendocrine phenotype.

In neuroblastoma, N-Myc, like c-Myc, is degraded via the ubiquitin-proteasome system upon phosphorylation at both S62 and T58 (Sjostrom et al., 2005). It has been previously shown that Aurora-A and N-Myc form a complex that results in N-Myc stabilization (Otto et al., 2009). Interestingly, this complex formation does not require Aurora-A catalytic activity (Otto et al., 2009). Most recently, it has been shown that Aurora-A also mediates c-Myc stability in *TP53*-altered hepatocellular carcinoma (Dauch et al., 2016). In our prostate cancer models, knockdown of Aurora-A using siRNA or treatment with the allosteric Aurora-A inhibitor MLN8237 resulted in decreased steady-state levels of N-Myc protein, decreased N-Myc target gene expression, and decreased cell viability. Altogether, our data shows the feasibility of exploiting the mutual dependence of N-Myc and Aurora-A to revert their oncogenic functions. Moreover, our data suggest that combination treatment targeting pathways associated with N-Myc-expressing prostate cancer (e.g., PI3K/AKT pathway inhibitors and EZH2 inhibitors) may provide synergy with allosteric Aurora-A inhibitors. Further in vivo validation for this is now warranted and may provide rationale for the clinical development of co-targeting approaches. Development of effective treatment strategies for patients with NEPC is a clinical unmet need.

One important finding from our study is that N-Myc represses AR signaling. One of the N-Myc downregulated AR targets is FKBP5, a member of the *cis-trans* prolyl isomerase or

immunophilin family of proteins (Ratajczak et al., 2003, 2015). FKBP5 serves as a scaffolding protein for AKT and PHLPP promoting PHLPP dephosphorylation of AKT at amino acid S473 (p-AKT). Mulholland et al. (2011) have shown that, in a mouse model of CRPC, FKBP5 is immediately suppressed after castration but upregulated upon hormone replacement in mouse prostates; downregulation of FKBP5 leads to activation of AKT by releasing FKBP5-PHLPP-mediated suppression of AKT. This was consistent with a previous report of crosstalk between androgen signaling and the PI3K pathway by Carver et al. (2011). Interestingly, we found that in the mouse model, MPC organoids, and LNCaP models, N-Myc protein levels were highly correlated with increased p-AKT protein levels and that N-Myc overexpressing cells are more sensitive to PI3K/AKT pathway inhibitors.

We found that N-Myc binds to AR enhancers and forms an interaction with the AR that is dependent on its interaction with EZH2. Further, the catalytic activity of EZH2 enhances N-Myc/AR/EZH2-PRC2 complex formation. We observed high levels of EZH2 protein levels and EZH2 activity in mouse models overexpressing N-Myc, and in human prostate cancer cells, N-Myc redirects EZH2 activity to N-Myc target gene promoters, which results in transcription repression, while EZH2 inhibition reverses N-Myc gene regulation. Moreover, N-Myc sensitizes cells to EZH2 inhibitors in vitro and in vivo. EZH2 has been implicated as a direct target gene of c-Myc in prostate cancer initiation (Koh et al., 2011). Whether N-Myc directly regulates EZH2 expression in late-stage prostate cancer remains to be determined. Moreover, there are likely other mechanisms involved as EZH2 is expressed in a higher frequency of CRPC cases than N-Myc. Nonetheless, our data suggest that N-Myc and EZH2 signaling are tightly linked in driving the NEPC molecular program. The interaction between N-Myc, AR, and EZH2 results in the abrogation of AR signaling despite abundant levels of AR, suggesting that the amplification of *MYCN* and loss of AR observed in NEPC tumor samples could be two independent events. The full extent of the role of N-Myc/EZH2 complex in regulating the AR pathway and other N-Myc target genes, the overlap between N-Myc and EZH2 genome occupancy, and the role of N-Myc and EZH2-mediated gene regulation through H3K27 methylation require further characterization. Interestingly, based on available ChIP-seq data from LNCaP cells, we noted that 85% ($p < 0.001$, permutation test) and 55% ($p = 0.03$, permutation test) of EZH2 and AR binding, respectively, contain N-Myc binding motifs, suggesting a genome-wide overlap between N-Myc and these other interacting proteins (Table S5). ChIP-seq for each of the proteins in the presence and absence of N-Myc binding will provide a more complete picture of genome-wide co-occupancy. Given the availability of EZH2 inhibitors that are now in phase 1 clinical trials for advanced solid tumors (e.g., NCT02082977), this characterization will potentially provide a rationale for further clinical development for patients with N-Myc-overexpressed NEPC and CRPC. Our data suggest that N-Myc expression and cooperation with EZH2 in CRPC might provide a selective advantage in the face of AR-directed therapy by shutting down AR signaling and establishing other pro-survival signaling pathways.

In summary, we show that N-Myc cooperates with EZH2 to drive the neuroendocrine phenotype in prostate cancer and provides rationale for targeted or co-targeting strategies for N-Myc-driven CRPC and the NEPC aggressive subgroup of late-stage prostate cancer.

EXPERIMENTAL PROCEDURES

Clinical Sample RNA-Seq Data Processing

The dataset included 178 CRPCs and 25 NEPCs. Of these tumor specimens, 34 CRPCs and 20 NEPCs were obtained and sequenced prospectively through clinical protocols approved by the WCM Institutional Review Board (IRB) with informed consent (IRB no. 1305013903, no. 1210013164) (Beltran et al., 2016). RNA-seq data for the remaining 144 CRPC and 5 NEPC cases were obtained through the SU2C-PCF clinical trial (Robinson et al., 2015), and data were accessed for this study through cBioPortal (Cerami et al., 2012).

Genetically Engineered Mouse Lines

All experimental procedures were carried out according to protocols approved by the WCM-IACUC (protocol no. 2008-0019).

Statistical Analysis

A Wilcoxon test was applied for mRNA differential analysis, followed by Benjamini-Hochberg correction for multiple hypothesis testing. Pearson correlation and the Fisher exact test were implemented for gene-gene expression correlation and genomic aberration association analysis, respectively. A Student's t test method was used to determine differences in tumor volumes in xenograft studies, with the criterion for significance <0.05.

ACCESSION NUMBERS

All RNA-seq and ChIP-seq data reported in this paper is GEO: GSE86532.

SUPPLEMENTAL INFORMATION

Supplemental Information includes Supplemental Experimental Procedures, seven figures, and five tables and can be found with this article online at http://dx.doi.org/10.1016/j.ccell.2016.09.005.

AUTHOR CONTRIBUTIONS

E.D., H.B., and D.S.R. designed, performed, and analyzed experiments. M.B., K.G., A.S., O.E., and F.D. performed bioinformatics analysis. H.B., M.A.R., and F.D. generated clinical RNA-seq data and annotated the patient samples. A.B. and L.P. performed and analyzed cell line experiments. C.C. generated all cell lines and performed experiments. J.C., Z.N., T.M., M.A.R., and J.-M.M. designed and performed RNAish experiments in GEM lines and clinical samples. J.C., J.-M.M., B.D.R., and M.A.R. performed pathology evaluations of all GEMs and clinical samples. D.O. and Y.C. developed mouse prostate organoid technology and worked with the Englander Institute for Precision Medicine, Weill Cornell Medicine (IPM-WCM) organoid platform and E.D. to establish GEM organoids for this manuscript. M.E. provided essential reagents. E.D., H.B., and D.S.R. wrote the manuscript. E.D., H.B., J.C., M.E., J.-M.M., B.D.R., O.E., M.A.R., F.D., and D.S.R. edited the manuscript. E.D. and H.B. share equal authorship.

Other details for the above and other experimental procedures are described in fully in Supplemental Experimental Procedures.

ACKNOWLEDGMENTS

We would like to gratefully thank Dr. Johannes Schulte (University of Essen, Essen, Germany and now at Charité – Universitätsmedizin Berlin) for providing the LSL-MYCN mouse for the generation of the GEM models described herein. We also would thank Chantal Pauli, Mirjam Blattner-Johnson, Jaclyn A. Croyle, and Sadia Mirza for their technical assistance and helpful comments and insights on data presented in the manuscript. We thank the following WCM core facilities: The Translational Research Program at WCM Pathology and Laboratory Medicine (Bing He, Yifang Liu, Leticia Dizon), the WCM-epigenomic core (Dr. Alicia Alonzo), the WCM-genomics resources core (Dr. Jenny

Xiang) facilities, and the IPM-WCM. This study was supported by the Prostate Cancer Foundation (PCF) Challenge award (D.S.R., M.E., H.B., M.R., O.E.) and the NIH (1R01CA179100-01A1) (D.S.R., O.E., J.-M.M., H.B.). This study was also supported in part by the Damon Runyon Cancer Research Foundation Clinical Investigator Award (CI-67-13) (H.B.), Department of Defense PC121341 (H.B.), Early Detection Research Network NCI U01 CA111275 (J.M.M. and M.A.R.), European Research Council ERCCoG648670 (F.D.), R01 CA116337 (H.B., F.D., M.A.R.) and by the Translational Research Program at WCM Pathology and Laboratory Medicine and a fellowship from the PhRMA Foundation (K.G.). L.P. is supported by an American-Italian Cancer Foundation Post-Doctoral Research Fellowship and PCF Young Investigator Award. Enzalutamide was provided by Astellas Pharma Inc. (Northbrook, IL) and Medivation, Inc. (San Francisco, CA). All EZH2 inhibitors were provided by GlaxoSmithKline (Newark, NJ). M.A.R. is listed as a co-inventor on a patent application for testing EZH2 in clinical samples (University of Michigan), which has been licensed to Ventana/Roche.

Received: December 11, 2015
Revised: June 22, 2016
Accepted: September 13, 2016
Published: October 10, 2016

REFERENCES

Althoff, K., Beckers, A., Bell, E., Nortmeyer, M., Thor, T., Sprussel, A., Lindner, S., De Preter, K., Florin, A., Heukamp, L.C., et al. (2015). A Cre-conditional MYCN-driven neuroblastoma mouse model as an improved tool for preclinical studies. Oncogene *34*, 3357–3368.

Beltran, H., Rickman, D.S., Park, K., Chae, S.S., Sboner, A., MacDonald, T.Y., Wang, Y., Sheikh, K.L., Terry, S., Tagawa, S.T., et al. (2011). Molecular characterization of neuroendocrine prostate cancer and identification of new drug targets. Cancer Discov. *1*, 487–495.

Beltran, H., Prandi, D., Mosquera, J.M., Benelli, M., Puca, L., Cyrta, J., Marotz, C., Giannopoulou, E., Chakravarthi, B.V., Varambally, S., et al. (2016). Divergent clonal evolution of castration-resistant neuroendocrine prostate cancer. Nat. Med. *22*, 298–305.

Brockmann, M., Poon, E., Berry, T., Carstensen, A., Deubzer, H.E., Rycak, L., Jamin, Y., Thway, K., Robinson, S.P., Roels, F., et al. (2013). Small molecule inhibitors of aurora-a induce proteasomal degradation of N-myc in childhood neuroblastoma. Cancer Cell *24*, 75–89.

Brognard, J., Sierecki, E., Gao, T., and Newton, A.C. (2007). PHLPP and a second isoform, PHLPP2, differentially attenuate the amplitude of Akt signaling by regulating distinct Akt isoforms. Mol. Cell *25*, 917–931.

Cancer Genome Atlas Research Network. (2015). The molecular taxonomy of primary prostate cancer. Cell *163*, 1011–1025.

Carver, B.S., Chapinski, C., Wongvipat, J., Hieronymus, H., Chen, Y., Chandarlapaty, S., Arora, V.K., Le, C., Koutcher, J., Scher, H., et al. (2011). Reciprocal feedback regulation of PI3K and androgen receptor signaling in PTEN-deficient prostate cancer. Cancer Cell *19*, 575–586.

Cerami, E., Gao, J., Dogrusoz, U., Gross, B.E., Sumer, S.O., Aksoy, B.A., Jacobsen, A., Byrne, C.J., Heuer, M.L., Larsson, E., et al. (2012). The cBio cancer genomics portal: an open platform for exploring multidimensional cancer genomics data. Cancer Discov. *2*, 401–404.

Chen, H., Sun, Y., Wu, C., Magyar, C.E., Li, X., Cheng, L., Yao, J.L., Shen, S., Osunkoya, A.O., Liang, C., and Huang, J. (2012). Pathogenesis of prostatic small cell carcinoma involves the inactivation of the P53 pathway. Endocr. Relat. Cancer *19*, 321–331.

Chen, Y., Chi, P., Rockowitz, S., Iaquinta, P.J., Shamu, T., Shukla, S., Gao, D., Sirota, I., Carver, B.S., Wongvipat, J., et al. (2013). ETS factors reprogram the androgen receptor cistrome and prime prostate tumorigenesis in response to PTEN loss. Nat. Med. *19*, 1023–1029.

Chesler, L., Schlieve, C., Goldenberg, D.D., Kenney, A., Kim, G., McMillan, A., Matthay, K.K., Rowitch, D., and Weiss, W.A. (2006). Inhibition of phosphatidylinositol 3-kinase destabilizes Mycn protein and blocks malignant progression in neuroblastoma. Cancer Res. *66*, 8139–8146.

Dauch, D., Rudalska, R., Cossa, G., Nault, J.C., Kang, T.W., Wuestefeld, T., Hohmeyer, A., Imbeaud, S., Yevsa, T., Hoenicke, L., et al. (2016). A MYC-aurora kinase A protein complex represents an actionable drug target in p53-altered liver cancer. Nat. Med. *22*, 744–753.

Gao, D., Vela, I., Sboner, A., Iaquinta, P.J., Karthaus, W.R., Gopalan, A., Dowling, C., Wanjala, J.N., Undvall, E.A., Arora, V.K., et al. (2014). Organoid cultures derived from patients with advanced prostate cancer. Cell *159*, 176–187.

Gao, D., Zhan, Y., Di, W., Moore, A.R., Sher, J.J., Guan, Y., Wang, S., Zhang, Z., Murphy, D.A., Sawyers, C.L., et al. (2016). A Tmprss2-CreERT2 knock-in mouse model for Cancer genetic studies on prostate and colon. PLoS One *11*, e0161084.

Grimmer, M.R., and Weiss, W.A. (2006). Childhood tumors of the nervous system as disorders of normal development. Curr. Opin. Pediatr. *18*, 634–638.

Gustafson, W.C., Meyerowitz, J.G., Nekritz, E.A., Chen, J., Benes, C., Charron, E., Simonds, E.F., Seeger, R., Matthay, K.K., Hertz, N.T., et al. (2014). Drugging MYCN through an allosteric transition in Aurora kinase A. Cancer Cell *26*, 414–427.

Hieronymus, H., Lamb, J., Ross, K.N., Peng, X.P., Clement, C., Rodina, A., Nieto, M., Du, J., Stegmaier, K., Raj, S.M., et al. (2006). Gene expression signature-based chemical genomic prediction identifies a novel class of HSP90 pathway modulators. Cancer Cell *10*, 321–330.

Humphrey, P.A. (2012). Histological variants of prostatic carcinoma and their significance. Histopathology *60*, 59–74.

Ito, T., Yamamoto, S., Ohno, Y., Namiki, K., Aizawa, T., Akiyama, A., and Tachibana, M. (2001). Up-regulation of neuroendocrine differentiation in prostate cancer after androgen deprivation therapy, degree and androgen independence. Oncol. Rep. *8*, 1221–1224.

Karthaus, W.R., Iaquinta, P.J., Drost, J., Gracanin, A., van Boxtel, R., Wongvipat, J., Dowling, C.M., Gao, D., Begthel, H., Sachs, N., et al. (2014). Identification of multipotent luminal progenitor cells in human prostate organoid cultures. Cell *159*, 163–175.

Khaw, Y.L., Nolan, N., Heaslip, I., McCormick, P.A., and Sheahan, K. (2011). Primary intrahepatic small-cell carcinoma arising from combined hepatocellular and cholangiocarcinomas. J. Clin. Oncol. *29*, e630–633.

Kim, K.H., Kim, W., Howard, T.P., Vazquez, F., Tsherniak, A., Wu, J.N., Wang, W., Haswell, J.R., Walensky, L.D., Hahn, W.C., et al. (2015). SWI/SNF-mutant cancers depend on catalytic and non-catalytic activity of EZH2. Nat. Med. *21*, 1491–1496.

Koh, C.M., Iwata, T., Zheng, Q., Bethel, C., Yegnasubramanian, S., and De Marzo, A.M. (2011). Myc enforces overexpression of EZH2 in early prostatic neoplasia via transcriptional and post-transcriptional mechanisms. Oncotarget *2*, 669–683.

Lee, J.K., Phillips, J.W., Smith, B.A., Park, J.W., Stoyanova, T., McCaffrey, E.F., Baertsch, R., Sokolov, A., Meyerowitz, J.G., Mathis, C., et al. (2016). N-myc drives neuroendocrine prostate Cancer initiated from human prostate epithelial cells. Cancer Cell *29*, 536–547.

Lotan, T.L., Gupta, N.S., Wang, W., Toubaji, A., Haffner, M.C., Chaux, A., Hicks, J.L., Meeker, A.K., Bieberich, C.J., De Marzo, A.M., et al. (2011). ERG gene rearrangements are common in prostatic small cell carcinomas. Mod. Pathol. *24*, 820–828.

Martin, P., Liu, Y.N., Pierce, R., Abou-Kheir, W., Casey, O., Seng, V., Camacho, D., Simpson, R.M., and Kelly, K. (2011). Prostate epithelial Pten/TP53 loss leads to transformation of multipotential progenitors and epithelial to mesenchymal transition. Am. J. Pathol. *179*, 422–435.

Mosquera, J.M., Beltran, H., Park, K., MacDonald, T.Y., Robinson, B.D., Tagawa, S.T., Perner, S., Bismar, T.A., Erbersdobler, A., Dhir, R., et al. (2013). Concurrent AURKA and MYCN gene amplifications are harbingers of lethal treatment-related neuroendocrine prostate cancer. Neoplasia *15*, 1–10.

Mott, L.J. (1979). Squamous cell carcinoma of the prostate: report of 2 cases and review of the literature. J. Urol. *121*, 833–835.

Mulholland, D.J., Tran, L.M., Li, Y., Cai, H., Morim, A., Wang, S., Plaisier, S., Garraway, I.P., Huang, J., Graeber, T.G., and Wu, H. (2011). Cell autonomous

role of PTEN in regulating castration-resistant prostate cancer growth. Cancer Cell *19*, 792–804.

Nelson, P.S., Clegg, N., Arnold, H., Ferguson, C., Bonham, M., White, J., Hood, L., and Lin, B. (2002). The program of androgen-responsive genes in neoplastic prostate epithelium. Proc. Natl. Acad. Sci. USA *99*, 11890–11895.

Otto, T., Horn, S., Brockmann, M., Eilers, U., Schuttrumpf, L., Popov, N., Kenney, A.M., Schulte, J.H., Beijersbergen, R., Christiansen, H., et al. (2009). Stabilization of N-Myc is a critical function of Aurora A in human neuroblastoma. Cancer Cell *15*, 67–78.

Parwani, A.V., Kronz, J.D., Genega, E.M., Gaudin, P., Chang, S., and Epstein, J.I. (2004). Prostate carcinoma with squamous differentiation: an analysis of 33 cases. Am. J. Surg. Pathol. *28*, 651–657.

Ratajczak, T., Cluning, C., and Ward, B.K. (2015). Steroid receptor-associated immunophilins: a gateway to steroid signalling. Clin. Biochem. Rev. *36*, 31–52.

Ratajczak, T., Ward, B.K., and Minchin, R.F. (2003). Immunophilin chaperones in steroid receptor signalling. Curr. Top Med. Chem. *3*, 1348–1357.

Robinson, D., Van Allen, E.M., Wu, Y.M., Schultz, N., Lonigro, R.J., Mosquera, J.M., Montgomery, B., Taplin, M.E., Pritchard, C.C., et al. (2015). Integrative clinical genomics of advanced prostate cancer. Cell *161*, 1215–1228.

Scheble, V.J., Braun, M., Beroukhim, R., Mermel, C.H., Ruiz, C., Wilbertz, T., Stiedl, A.C., Petersen, K., Reischl, M., Kuefer, R., et al. (2010). ERG rearrangement is specific to prostate cancer and does not occur in any other common tumor. Mod. Pathol. *23*, 1061–1067.

Schlaeger, C., Longerich, T., Schiller, C., Bewerunge, P., Mehrabi, A., Toedt, G., Kleeff, J., Ehemann, V., Eils, R., Lichter, P., et al. (2008). Etiology-dependent molecular mechanisms in human hepatocarcinogenesis. Hepatology *47*, 511–520.

Shachaf, C.M., Kopelman, A.M., Arvanitis, C., Karlsson, A., Beer, S., Mandl, S., Bachmann, M.H., Borowsky, A.D., Ruebner, B., Cardiff, R.D., et al. (2004). MYC inactivation uncovers pluripotent differentiation and tumour dormancy in hepatocellular cancer. Nature *431*, 1112–1117.

Shen, R., Dorai, T., Szaboles, M., Katz, A.E., Olsson, C.A., and Buttyan, R. (1997). Transdifferentiation of cultured human prostate cancer cells to a neuroendocrine cell phenotype in a hormone-depleted medium. Urol. Oncol. *3*, 67–75.

Sjostrom, S.K., Finn, G., Hahn, W.C., Rowitch, D.H., and Kenney, A.M. (2005). The Cdk1 complex plays a prime role in regulating N-myc phosphorylation and turnover in neural precursors. Dev. Cell *9*, 327–338.

Small, E.J., Aggarwal, R.R., Huang, J., Sokolov, A., Zhang, L., Alumkal, J.J., Youngren, J., Ryan, C.J., Foye, A., Reiter, R.E., et al. (2016). Clinical and genomic characterization of metastatic small cell/neuroendocrine prostate cancer (SCNC) and intermediate atypical prostate cancer (IAC): results from the SU2C/PCF/AACRWest Coast Prostate Cancer Dream Team (WCDT). J. Clin. Oncol. *34* (suppl), abstr 5019.

Tan, H.L., Sood, A., Rahimi, H.A., Wang, W., Gupta, N., Hicks, J., Mosier, S., Gocke, C.D., Epstein, J.I., Netto, G.J., et al. (2014). Rb loss is characteristic of prostatic small cell neuroendocrine carcinoma. Clin. Cancer Res. *20*, 890–903.

Wang, H.T., Yao, Y.H., Li, B.G., Tang, Y., Chang, J.W., and Zhang, J. (2014). Neuroendocrine prostate Cancer (NEPC) progressing from conventional prostatic adenocarcinoma: factors associated with time to development of NEPC and survival from NEPC diagnosis-a systematic review and pooled analysis. J. Clin. Oncol. *32*, 3383–3390.

Williamson, S.R., Zhang, S., Yao, J.L., Huang, J., Lopez-Beltran, A., Shen, S., Osunkoya, A.O., MacLennan, G.T., Montironi, R., and Cheng, L. (2011). ERG-TMPRSS2 rearrangement is shared by concurrent prostatic adenocarcinoma and prostatic small cell carcinoma and absent in small cell carcinoma of the urinary bladder: evidence supporting monoclonal origin. Mod. Pathol. *24*, 1120–1127.

Wright, M.E., Tsai, M.J., and Aebersold, R. (2003). Androgen receptor represses the neuroendocrine transdifferentiation process in prostate cancer cells. Mol. Endocrinol. *17*, 1726–1737.

Wu, X., Wu, J., Huang, J., Powell, W.C., Zhang, J., Matusik, R.J., Sangiorgi, F.O., Maxson, R.E., Sucov, H.M., and Roy-Burman, P. (2001). Generation of a prostate epithelial cell-specific Cre transgenic mouse model for tissue-specific gene ablation. Mech. Dev. *101*, 61–69.

Xu, K., Wu, Z.J., Groner, A.C., He, H.H., Cai, C., Lis, R.T., Wu, X., Stack, E.C., Loda, M., Liu, T., et al. (2012). EZH2 oncogenic activity in castration-resistant prostate cancer cells is Polycomb-independent. Science *338*, 1465–1469.

Yuan, T.C., Veeramani, S., Lin, F.F., Kondrikou, D., Zelivianski, S., Igawa, T., Karan, D., Batra, S.K., and Lin, M.F. (2006). Androgen deprivation induces human prostate epithelial neuroendocrine differentiation of androgen-sensitive LNCaP cells. Endocr. Relat. Cancer *13*, 151–167.

Zhang, W., Yu, Y., Hertwig, F., Thierry-Mieg, J., Zhang, W., Thierry-Mieg, D., Wang, J., Furlanello, C., Devanarayan, V., Cheng, J., et al. (2015). Comparison of RNA-seq and microarray-based models for clinical endpoint prediction. Genome Biol. *16*, 133.

Zhou, Z., Flesken-Nikitin, A., Corney, D.C., Wang, W., Goodrich, D.W., Roy-Burman, P., and Nikitin, A.Y. (2006). Synergy of p53 and Rb deficiency in a conditional mouse model for metastatic prostate cancer. Cancer Res. *66*, 7889–7898.